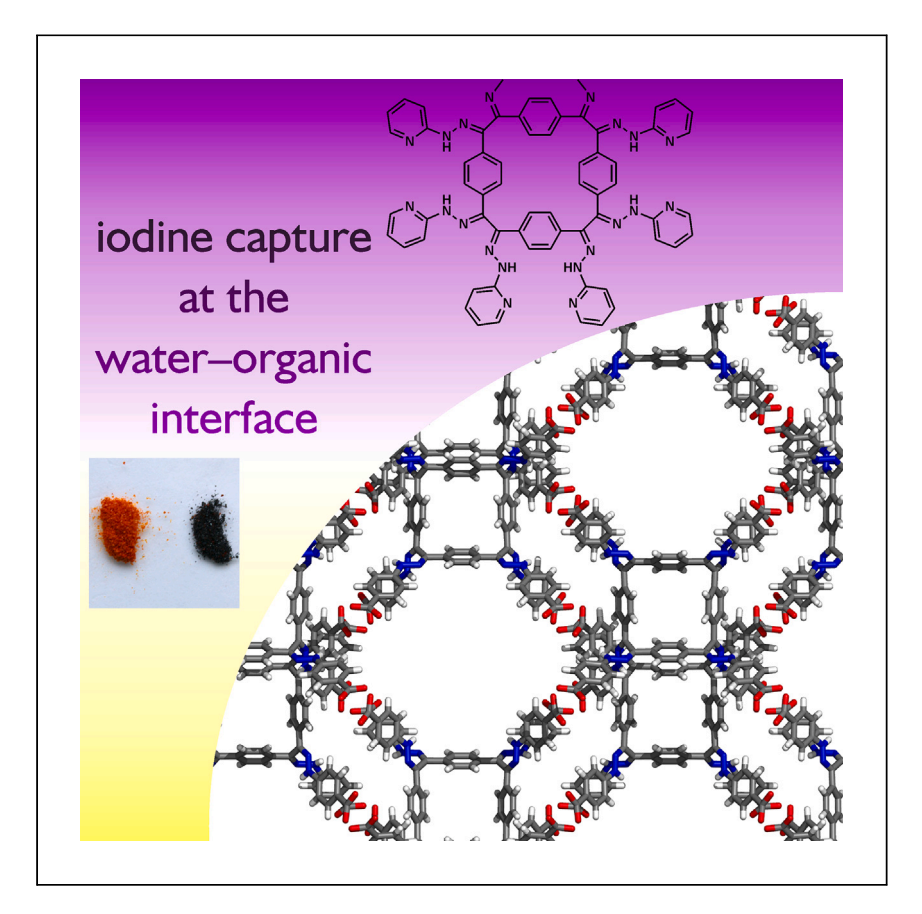


### **Article**

# Cyclobenzil hydrazones with high iodine capture capacities in solutions and on interfaces



Robles et al. report the facile preparation and structural analysis of five hydrazones based on the cyclotetrabenzil scaffold. These materials' crystal structures progressively open as the interactions holding them change from aromatic stacking to hydrogen bonding. One of the prepared molecules shows exceptional iodine uptake capacity for a molecular material.

Alexandra Robles, Maymounah Alrayyani, Xiqu Wang, Ognjen Š. Miljanić

miljanic@uh.edu

### Highlights

Five cyclotetrabenzil octahydrazones are prepared in high yield

Their crystal packing is mediated by hydrogen bonding and aromatic stacking

Pyridine-based system shows very high iodine uptake for a nonpolymeric material

Robles et al., Cell Reports Physical Science 4, 101509

August 16, 2023 © 2023 The Author(s). https://doi.org/10.1016/j.xcrp.2023.101509





### **Article**

# Cyclobenzil hydrazones with high iodine capture capacities in solutions and on interfaces

Alexandra Robles, <sup>1</sup> Maymounah Alrayyani, <sup>1,2</sup> Xiqu Wang, <sup>1</sup> and Ognjen Š. Miljanić <sup>1,3,\*</sup>

### **SUMMARY**

Porous molecular crystals (PMCs) are solution-processable materials with promising applications in thin films and devices. However, some PMCs are only virtually porous, as their pores collapse when desolvated. We demonstrate the productive use of virtual porosity when non-volatile I2 guest acts as the probe. We prepared a series of cyclotetrabenzil hydrazones with progressively larger cavities. Their measured surface areas of up to 131 m<sup>2</sup> g<sup>-1</sup> are negligible compared with the values predicted from crystal structures. Nevertheless, they effectively capture I<sub>2</sub> from aqueous and organic media and at the organic-aqueous interface, with capture capacities scaling with virtual void volumes. The pyridine-functionalized system is a notable outlier, engaging up to 21 I<sub>2</sub> molecules and showing capture capacity of 4.15 g g<sup>-1</sup>, unprecedented among non-polymeric materials. These findings could impact the management of radioactive I<sub>2</sub> and help in ensuring the integrity of protective coatings of nuclear reactors and waste containment vessels.

### INTRODUCTION

With the ever-increasing environmental and geopolitical concerns about fossil fuel use, nuclear energy is a subject of renewed interest as the only currently scalable and geographically unrestricted way of producing electricity without greenhouse gas emissions. 1,2 To alleviate public concerns about safety, comprehensive strategies for the management of nuclear waste must be developed.<sup>3</sup> Radioactive iodine isotopes I-131 (half-life,  $\tau_{1/2}$  = 8 days) and I-132 ( $\tau_{1/2}$  = 3 days) are common products of nuclear fission and have been implicated in spreading the radioactivity following the Chernobyl accident. Iodine's volatility, solubility in organic and aqueous media, and tendency to concentrate in the human thyroid gland all make it a problematic pollutant. Radioactive iodine additionally damages the nuclear paint used to coat the insides of nuclear reactors and waste containment vessels.<sup>5</sup> Through incompletely understood mechanisms that involve radical formation and iodination of residual solvents in paint formulations, radioactive irradiation of these paints yields small and volatile organic alkyl iodides, more difficult to capture than the iodine itself. As nuclear paints are hydrophobic, stopping iodine transfer from the aqueous to the organic layer can be a viable strategy for preventing this significant contamination problem.

Porous metal-organic (MOFs)<sup>6</sup> and covalent organic frameworks (COFs),<sup>7,8</sup> and porous organic polymers have all been studied as iodine capture materials.<sup>9</sup> While some showed high uptake capacities, the polymeric nature of these materials makes them insoluble and difficult to deposit at interfaces or use as coatings. Here, we report alternative, high-performing molecular iodine capture materials, which (1) are solution processable and thus easily adapted to paintable coatings, (2) show



<sup>&</sup>lt;sup>1</sup>Department of Chemistry, University of Houston, 3585 Cullen Boulevard 112, Houston, TX 77204-5003, USA

<sup>&</sup>lt;sup>2</sup>Chemistry Department, King Abdulaziz University, Jeddah 23218, Saudi Arabia

<sup>3</sup>Lead contact

<sup>\*</sup>Correspondence: miljanic@uh.edu https://doi.org/10.1016/j.xcrp.2023.101509



Scheme 1. Synthesis of cyclotetra(bisarylhydrazone)benzils 1a-e

iodine uptake capacities of up to  $4.15 \text{ g g}^{-1}$ , comparable to COFs<sup>8</sup> and unprecedented among small molecules, and (3) can capture iodine at critical water-organic solvent interfaces. These molecular crystals are based on the readily prepared cyclotetrabenzil hydrazones 1a-e (Scheme 1).

### **RESULTS AND DISCUSSION**

### **Synthesis**

Cyclotetra(bisarylhydrazone)benzils 1a—e were synthesized by 8-fold hydrazone condensations between cyclotetrabenzil (3) $^{10}$  and arylhydrazines 2a—e in EtOH, PhMe, or p-xylene as the solvents and with p-toluenesulfonic acid as the catalyst (Scheme 1). The desired hydrazone products were isolated as crystalline solids in yields between 49% and 90%, corresponding to per-condensation yields ranging from 91.5% (1a) to 98.7% (1d). $^{11}$ 

### **Spectroscopic characterization**

Spectroscopic characterization data of 1a-e are consistent with their molecular structures. The effects of the bulky aryl substituents on the conformational dynamics of 1a-e in solution were probed by variable-temperature <sup>1</sup>H NMR spectroscopy. At ambient conditions, two broad singlets are associated with the phenylene protons of the macrocyclic skeleton in 1a and 1c-e (Figures S17-S29; compound 1b was not studied because of insolubility in all deuterated solvents of sufficiently high boiling point). This doubling up of peaks can be caused either by the slow rotation of the phenylene moieties of the central macrocycle around their C1-C4 axes, or by the slow slipping of the neighboring hydrazine arms by each other. At the coalescence temperatures  $(T_c)$ , the rate constants  $(k_c)$  for the dynamic processes were calculated using the Gutowsky-Hold equation,  $k_c = 2.22\Delta v$ , where  $\Delta v$  represents the difference in chemical shifts between the phenyl hydrogens in the macrocylic skeleton. The Gibbs free energies of activation ( $\Delta G^{\dagger}$ ) were calculated, assuming unity in the transmission coefficient ( $\kappa$ ), using the Eyring equation,  $\Delta G^{\ddagger} = RT_c[\ln T_c - \ln k_c + 23.76]$ . <sup>12</sup> The results of the variable-temperature <sup>1</sup>H NMR studies of the conformational dynamics of cyclotetra(bisarylhydrazone)benzils are summarized in Table 1 and Figures S30-S33.



Table 1. Calculated rate constants ( $k_c$ ) and Gibbs' activation energies ( $\Delta$   $G^{\ddagger}$ ) for conformational equilibration of compounds 1a–e in DMSO- $d_6$ 

Compound	$\delta$ , (Hz) <sup>a</sup>	T <sub>c</sub> , (K)	$k_c$ , (s <sup>-1</sup> )	$\Delta G^{\dagger}$ , (kcal mol <sup>-1</sup> )
1a	4,110, 4,730	323	1,376	14.35
1c	4,003, 4,925	319	2,048	13.91
1d	4,001, 4,996	315	2,209	13.68
1e	3,972, 4,966	310	2,223	13.45

 $<sup>^{\</sup>mathrm{a}}$ The  $^{\mathrm{1}}$ H NMR chemical shifts of the macrocycle skeleton phenyl ring protons are shown in Hz. Spectrometer frequency: 600 MHz for  $^{\mathrm{1}}$ H nuclei.

The inversion barriers for 1a-e proved minimally sensitive to substitution. This observation suggests that the barriers are largely steric in nature, as the four studied molecules have pendant hydrazone groups of similar sizes. Indirectly, it may also point to the free rotation of the phenylene rings in the central core as the equilibrating process—since the bypassing of the hydrazone arms would involve planarization in the transition state and would thus probably be sensitive to electronic effects.

### **Crystallographic characterization**

Single crystals of 1a–e were grown by slow vapor diffusion and analyzed by X-ray diffraction (Tables 2, S1–S5, and Figures S1–S5). While the crystals of 1a–d were grown under routine conditions, hydrazone 1e was crystallized by vapor diffusion of a 0.2 M solution of  $l_2$  in acetone into a 0.05 M solution of 1e in tetrahydrofuran (THF). These unusual crystallization conditions were critical, as numerous prior attempts using various solvent combinations produced crystals of insufficient quality for X-ray diffraction. To our surprise, iodine was not incorporated into the crystal structure of 1e when its large yellow prismatic crystals were harvested after 7 days.

As Figure 1 shows, all five derivatives maintain the roughly square-shaped central cavity (see also Table S8). A closer inspection of their dimensions revealed that the macrocyclic scaffolds adopt boat-like conformations with the directions of opposing dihedral angles being the same (see Figure 1 and Tables S1–S6). In all prepared octahydrazones, the two immediately adjacent arylhydrazone arms point in the opposite directions, while those separated by the phenylene rings point in the same direction, resulting in an overall ab-ba-ab-ba arrangement (where "a" describes units positioned above the plane of the central macrocycle and "b" those positioned below the plane). The C=N bonds are in the (Z)-configuration, and the C=N-NH-Ar linkers are in the extended zigzag conformation. In 1a–d, C=N bonds are shorter (1.28–1.34 Å) than the N-N (1.34–1.37 Å) bonds, consistent with the hydrazone tautomer. However, in 1e, this trend in bond lengths switches in four out of eight C=N-NH moieties; this observation is counterintuitive as the electron-withdrawing –COOH group should shorten the Ar–N and N=C bonds, lengthening the central N-N bond in hydrazones.

While the molecular structures of 1a–e appear very similar, their extended crystal structures (Figure 2) greatly differ, progressively opening up along the series. Compound 1a forms the most tightly packed structure with solvent-accessible void volume of 25.3% of the total unit cell. In 1b, this void volume increased to 33.3%. Compound 1c crystallizes with eight AcOH molecules per unit cell. It is the only crystal structure in the series that includes ordered solvent molecules: the AcOH molecule establishes  $[O-H\cdots N]$  (2.10 Å) and  $[N-H\cdots O]$  (1.78 Å) hydrogen bonds with the 2-hydrazonopyridine moiety of 1c. Its void volume is



Table 2. Vapor diffusion crystal growth conditions and key parameters for 1a-e								
Compound	Solvent	Crystal description	Time (days)	Space group	Z			
1a	hexane into CHCl <sub>3</sub>	yellow, needle-shaped	3	P1	2			
1b	EtOH into CHCl <sub>3</sub>	yellow, needle-shaped	5	P2 <sub>1</sub> /n	4			
1c·2AcOH	Et <sub>2</sub> O into AcOH	yellow, prismatic	2	P2/c	2			
1d	hexane into THF	red, needle-shape	3	P42 <sub>1</sub> /c	6			
1e	$0.2~\mathrm{M}$ solution of $\mathrm{I}_2$ in acetone into THF	yellow, prismatic	7	<i>P</i> mna	6			

38.1%. The final two structures of 1d and 1e were characterized by the solvent-accessible void volumes of 53.1% and 79.1%, respectively. Disappointingly, these large voids are not persistent: exposed to air, the crystals collapsed within minutes. An analysis of such minimally crystalline powders for 1c and 1e revealed Brunauer-Emmett-Teller surface areas of just 24.1 and 131 m² g $^{-1}$ , respectively (Figures S6 and S7, respectively). These values are similar to those measured for the parent cyclotetrabenzoin but far below the theoretical values of up to 3,531 m² g $^{-1}$  for 1e (calculated using Materials Studio). Thus, structures of 1a–e are only *virtually* porous as defined by Barbour.  $^{15}$ 

### **lodine capture experiments**

Inspired by the crucial role iodine played in the successful crystallization of 1e, we decided to investigate whether these cyclotetra(bisarylhydrazone)benzils could uptake iodine within their nitrogen-rich structures. Initial experiments to probe their adsorption capabilities were carried out using I2 vapor at room temperature. Exposing all five derivatives 1a-e, as well as the parent cyclotetrabenzoin (6) and cyclotetrabenzil (3), to I<sub>2</sub> vapor led to an increase in their mass as a function of time (Figure 3, left), and to the darkening of the compounds' colors (Figure 3, top right). The non-functionalized parent compounds 6 and 3 adsorbed virtually no I2, having capacities of 0.065 and  $0 \text{ g g}^{-1}$ , respectively. The adsorption profiles of compounds 1a, 1b, 1d, and 1e followed an almost linear initial trend, which began to plateau after 5 days, signaling that equilibrium had been reached. Final uptake capacities correlated with the observed void volumes: the lowest one for 1a, slightly higher for 1b and 1d, and the highest seen for 1e. However, the uptake capacity of 1c did not reach equilibrium until day 20 and demonstrated an outstandingly high capacity of 4.15 g  $g^{-1}$ , which equates to  $\sim$ 21 molecules of  $I_2$  per molecule of 1c (Figure 3).

We extended the study to examine the ability of 1c to uptake  $I_2$  from solutions in organic solvents and water. When 1c was introduced into a 1 mM solution of  $I_2$  in hexane, a rapid decrease of ~70% of  $I_2$  concentration was observed in the UV/Vis absorption spectrum and was accompanied by the fading of the purple color of the solution (Figures S10 and S11A). The adsorption rate gradually decreased until most of  $I_2$  was removed after 30 h. Compound 3 and the monomeric model compound benzil-bis-2-pyridinylhydrazone (4) did not have a significant effect on the concentration of  $I_2$ , and hydrazone 4 begun dissolving in hexane after 2 h (Figure S12). In aqueous media, we investigated two different systems: Lugol's triodide solution prepared using  $I_2$  and KI and a solution of  $I_2$  that was allowed to oxidize in water for 3 days to produce hypoiodate. These two solutions are relevant to the photochemical speciation of radioiodine, which produces various iodine species that have been detected in nuclear waste and nuclear accidents.  $^{16,17}$  The addition of 1c into these two 1 mM aqueous iodine solutions led



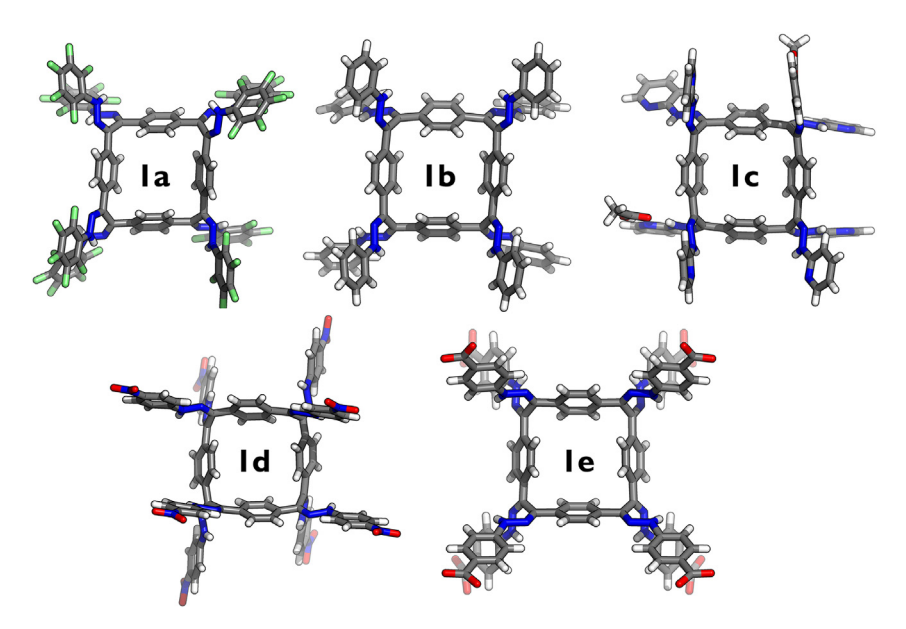


Figure 1. Molecular structures of cyclotetrabenzil octahydrazones
Crystal structures of 1a–e. Element colors: C, gray; H, white; O, red; N, blue; F, lime.

to approximately 60% and 70% respective decreases in  $I_2$  concentration over 6 h (Figures S10 and S11B). From these experiments, we concluded that the adsorption efficiency of 1c can be simultaneously attributed to its rigidity, virtual porosity, and hydrazine functionalization. The non-functionalized cyclotetrabenzil (3) adsorbed virtually no  $I_2$  in solution, while the monomeric 4 suffered from high solubility in organic solvents, making it unsuitable for adsorption in such media. Approximately 85% of the iodine adsorbed within 1c could be released by submerging  $I_2@1c$  powder in 1,4-dioxane for 24 h (Figure S13), and the sample can be recycled (Figures S14 and S15).

Finally, we tested whether the  $I_2$  adsorption could occur at an organic-aqueous interface as shown in Figure 3, bottom right (see also Figure S16). Compound 1c is hydrophobic—as evidenced by the water contact angle of 87° (Figure S34)—and apparently has lower density than water, which results in its deposition on the interface between the organic and aqueous layers. In that interlayer position, 1c can successfully adsorb  $I_2$  from either the hexane or the water layer. In addition, having 1c laid in between the two media creates a protective coating that prevents  $I_2$  from diffusing between the organic and aqueous layers. This feature is particularly important for nuclear waste treatment: organic iodides in nuclear waste containment tanks are formed by the interaction of iodine-containing water droplets with the petroleumbased paints covering the inside of these containment tanks. Organic iodides are highly volatile and toxic,  $^{18}$  and preventing contact between iodine in aqueous media with organic substances could ameliorate the formation of these species. To our knowledge, this is the first example of iodine adsorption tested between two immiscible liquid phases.

### Crystal structures of 1a-e

The crystal structures of 1a–e show distinct opening along the series, with a marked increase in the solvent-accessible void volume. These changes in the overall packing pattern are consequences of the changes in the dominant noncovalent interaction



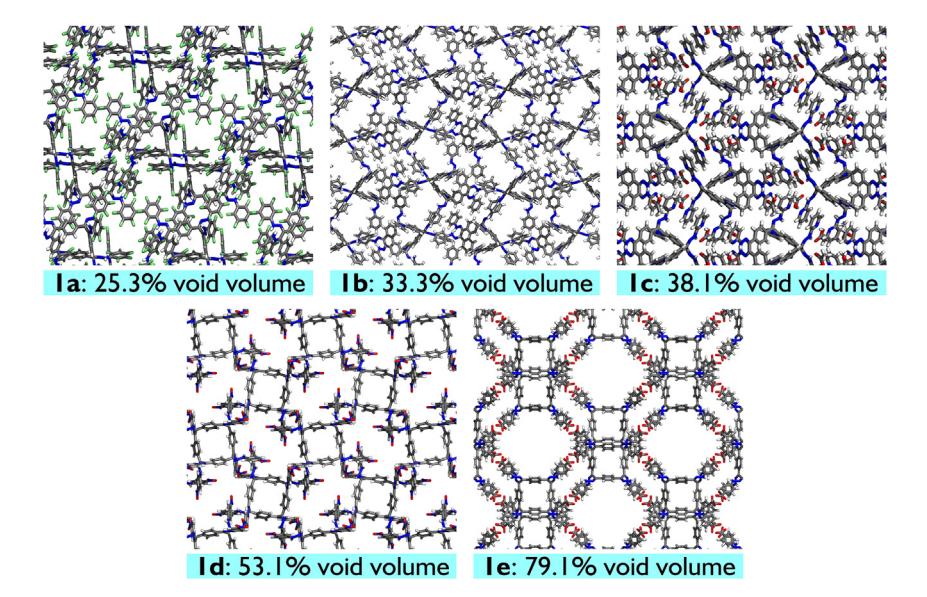


**Figure 2. Crystal packing diagrams**Segments of extended packing diagrams of 1a–e, along with their crystallographically determined void volumes. Element colors: C, gray; H, white; O, red; N, blue; F, lime.

that stabilizes the extended structures along the series. In the most tightly packed structure of 1a, the key stabilizing interaction is the  $[\pi\cdots\pi]$  stacking between the phenyl rings of the macrocycle and the pentafluorophenyl rings (Figure 4) of four neighboring molecules, with centroid-to-centroid distances between 3.55 and 3.57 Å. <sup>19</sup> These neighbors arrange themselves synclinally around the scaffold with two opposite pairs rotated clockwise with [N=C-C=N] dihedral angles of 58.3° and 60.0° and the other two opposite pairs rotated counterclockwise with dihedral angles of  $-71.3^\circ$  and  $-76.7^\circ$ . Out of the eight pentafluorophenyl arms on each molecule of 1a, only four engage in aromatic stacking with the macrocyclic core. The other four instead establish [C-F···F], [F-C···C], and [C-H···N] short contacts ranging in length from 2.29 to 3.45 Å.

Similar close packing behavior was observed in compound 1b. Four molecules surround each central structure in a synclinal stereochemical arrangement with two opposite pairs rotated clockwise with the [N=C-C=N] dihedral angles measuring 72.1° and 77.1° and the two other opposite pairs rotated counterclockwise with dihedral angles of  $-78.6^{\circ}$  and  $-89.8^{\circ}$ . Notable are T-shaped [C-H··· $\pi$ ] interactions (Figure 4) between the pendant phenyl rings and between the phenyl rings of the macrocycle with pendant arms, with [C-H··· $\pi$ ] distances measuring between 2.56 and 2.68 Å, consistent with the previously reported values. Phenyl rings of the hydrazone arms also approach each other in a rather unconvincing [ $\pi$ ··· $\pi$ ] stacking arrangement, characterized by the shortest [C···C] contact of 3.21 Å, centroid-centroid distance of 4.66 Å, and an interplanar angle of 14.4°.

In the extended structure of  $1c \cdot 2AcOH$ , each molecule is surrounded by four neighbors arranged in an anticlinal fashion with two opposite pairs rotated in a clockwise direction having identical [N=C-C=N] dihedral angles of 90.9° and the other two opposite pairs rotated counterclockwise, with dihedral angles of  $-110.2^{\circ}$  and  $-107.7^{\circ}$ . Once again, the extended crystal structure is dominantly stabilized by  $[\pi \cdots \pi]$  interactions but now exclusively between the pendant arms bearing pyridyl rings: the aromatic rings of the central core are no longer involved (Figure 4). The



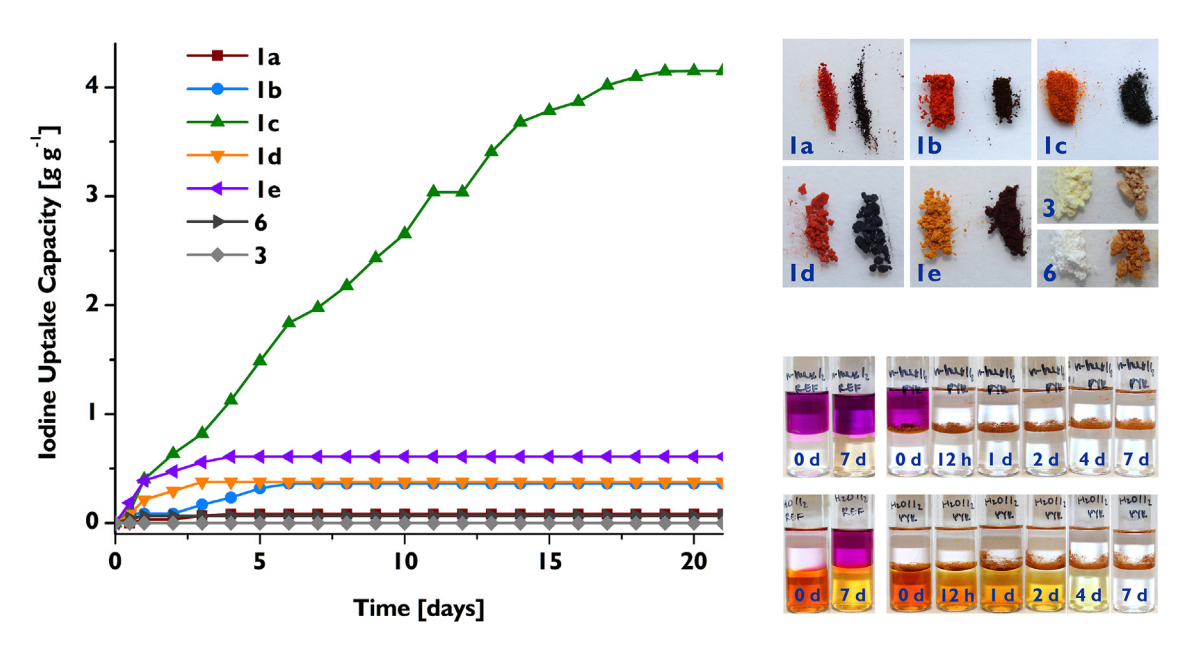


Figure 3. Iodine uptake studies
Left: plot of  $I_2$  vapor uptake by hydrazones 1a–e, cyclotetrabenzil (3), and cyclotetrabenzoin (6) as a function of adsorption time. Top right: color changes observed upon exposure of 1a–e, 3, and 6 to  $I_2$  vapor. Bottom right: hydrazone 1c deposited in the powder form on the organic/aqueous interface prevents  $I_2$  migration from hexane to water (top row of photographs) and vice versa (bottom row); two leftmost photos in each row are control experiments without 1c.

centroid-to-centroid distances in the antiparallel pyridyl  $[\pi\cdots\pi]$  stacks alternate between 3.57 and 3.78 Å, in line with the literature precedent. Several additional short contacts, ranging in length from 2.30 to 3.39 Å, are observed in the extended structure.

In the nitro-functionalized 1d, the extended crystal structure is held together by a combination of  $[\pi\cdots\pi]$  stacking and hydrogen bonding. The 4-nitrophenyl moieties from two neighboring molecules of 1d engage into slipped  $[\pi\cdots\pi]$  interactions with centroid-to-centroid distances of 3.68 Å (Figure 4). This interaction brings the  $-NO_2$  groups close enough to the hydrazone's NH moieties to allow the establishment of two  $[N-H\cdots O-N]$  hydrogen bonds characterized by  $[O\cdots H]$  distances of 2.16 and 2.17 Å. An additional short contact measuring 2.54 Å is observed between the nitro group and a hydrogen on the central macrocyclic core. The packed structure contains one intrinsic pore created by the cyclotetrabenzil central cavity as well as two extrinsic pores, one of which is shown in Figure 2. The neighboring molecules are arranged in a synclinal fashion with two opposite pairs rotated clockwise with [N=C-C=N] dihedral angles of 178.18° and 171.07°, while the other two opposite pairs are rotated counterclockwise and have identical dihedral angles of -178.18°.

The structure of 1e forms a three-dimensional hydrogen-bonded network, within which every 4-carboxyphenylhydrazone moiety interacts with one arm of a neighboring molecule through a head-on carboxylic acid dimer interaction, as shown on a fragment in Figure 4, far right. All heavy atom  $[O\cdots O]$  contacts within hydrogen-bonded dimers measure between 2.58 and 2.66 Å. This association pattern leads to a highly porous structure with several visible pores along all three crystallographic axes, two of which can be seen in Figure 2. Oligocarboxylic acids such as 1e have been used to construct MOFs with interesting topologies  $^{25,26}$  and excellent performance in gas separation and ion sensing.  $^{27-30}$  Compound 1e stands apart from



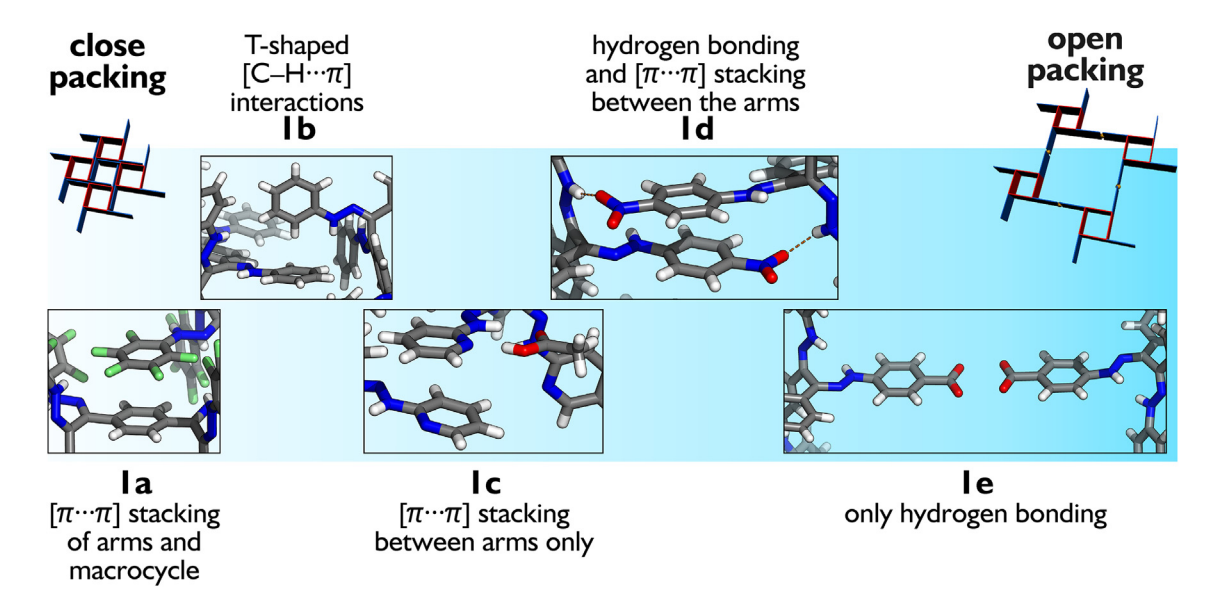


Figure 4. Progressive opening of the extended structures in the octahydrazone series

Highlights of key noncovalent interactions stabilizing the extended crystal structures of 1a–e. Element colors: C, gray; H, white; O, red; N, blue; F, lime.

other octacarboxylic acid MOF precursors as the only truly octapodal in nature. <sup>25,26</sup> The largest virtual pore in the extended structure of 1e has a diameter of 30 Å— almost as large as the record for the largest void in a hydrogen-bonded organic framework based on an oligocarboxylic acid, measuring 31.2 Å. <sup>31,32</sup> Its theoretical surface area rivals some of the highest measured for PMCs. <sup>33,34</sup>

### lodine capture performance of 1a-e

The  $I_2$  uptake in 1c is 64-fold higher than the capacity exhibited by 6, surpassing that of the adaptive bypiridine cage reported by Sessler that previously held the record for  $I_2$  uptake in a seemingly non-porous compound (Table S7), <sup>35</sup> and it is comparable to uptakes by polymeric materials. <sup>7,8</sup> The exposed electron-rich nitrogen-containing groups of the arm moieties play a critical role strengthening the interactions between the host macrocycle 1c and  $I_2$ . <sup>1</sup>H NMR titration experiments (Figure S8) support the interactions of the electron-rich pyridine and amine subunit of the hydrazone bridge with  $I_2$ ; as the  $I_2$  loading was increased, there was a downfield shift of the aromatic protons corresponding to the pyridine heterocycle and the –NH proton. Similar interactions of iodine in nitrogen-rich systems have been reported by Sessler, <sup>35</sup> Wang, <sup>36</sup> and Li. <sup>37</sup> Furthermore, the FT-IR spectra of 1c and  $I_2$ @1c are consistent with this conclusion as the characteristic peaks of ~1,640 cm<sup>-1</sup> and ~3,312 cm<sup>-1</sup> assigned to the C=N and N-H stretches, respectively, decrease in intensity following exposure to  $I_2$  but recover after desorption of the guest (Figure S9).

In conclusion, starting from the common cyclotetrabenzil precursor, five octahydrazones were prepared and thoroughly studied by crystallography and spectroscopy. The most closely packed structure of 1a followed Kitaigorodskii's principle by dovetailing its electron-poor fluorinated pendant chains with the electron-rich central macrocycle. As the electronic nature of the pendant groups changed to be more electron rich in 1b and 1c, this interaction became less favorable, and the structures started opening. Finally, the introduction of weakly (in 1d) and strongly (in 1e) hydrogen-bonding groups further weakened the  $[\pi \cdots \pi]$  stacking interactions and eventually led to a completely opened hydrogen-bonded structure of 1e. This

### **Article**



fine-tuning of crystal packing was easily accomplished: hydrazones are prepared in a single high-yielding step and are famed for their crystallinity. 38,39

All five hydrazones' structures exhibit only virtual porosity: once exposed to air, they quickly lose their disordered solvents. However, when exposed to iodine guest, this virtual porosity has real consequences: their iodine capture capacities roughly scaled with the crystallographically observed void volumes. An exception to this trend was compound 1c, whose nitrogen-based functional groups showed much higher I<sub>2</sub> capture affinity that those in other systems. Here too, virtual porosity was effectively turned on by the presence of the nitrogen-based groups, which allowed dramatic increase in the iodine capture capacities. The resulting uptake was the highest among the reported molecular materials and comparable to the porous COFs, with the added benefit of solution processability of 1c.

Future work in our group will explore (1) the kinetics of structural opening along the 1a–e series, (2) the behavior of these structures at elevated pressures, (3) the stability of 1c and its congeners to radioactive iodine, and finally (4) mechanism of I<sub>2</sub> inclusion within the structure of 1c. The results of these studies will be reported in due course.

#### **EXPERIMENTAL PROCEDURES**

### Resource availability

#### Lead contact

Further information and requests for resources should be directed to and will be fulfilled by the lead contact, Ognjen Š. Miljanić (miljanic@uh.edu).

### Materials availability

Most materials generated in this study are available from the lead contact upon request.

### Data and code availability

Crystallographic data for compounds 1a–e were deposited in the Cambridge Crystallographic Data Center under deposition codes 2164631 and 2164803–2164806. Further experimental details are provided in the supplemental experimental procedures.

### **SUPPLEMENTAL INFORMATION**

Supplemental information can be found online at https://doi.org/10.1016/j.xcrp. 2023.101509.

### **ACKNOWLEDGMENTS**

This work was supported by the National Science Foundation (CHE-2204236 to O.Š.M.) and the donors of the American Chemical Society Petroleum Research Fund (award 58919-ND4 to O.Š.M.). O.Š.M. gratefully acknowledges the support from the Alexander von Humboldt Foundation for his sabbatical stay at the Ruprecht-Karls-Universität Heidelberg (Germany), where parts of this manuscript were written.

### **AUTHOR CONTRIBUTIONS**

A.R. and M.A. prepared and characterized 1a–e. A.R. designed and performed all iodine capture experiments. X.W. solved the crystal structures of 1a–e. O.Š.M. and A.R. wrote the article, incorporating suggestions of all coauthors.





#### **DECLARATION OF INTERESTS**

Preliminary invention disclosure had been filed on this work: Miljanić, O. Š.; Robles, A. Novel Material for Iodine Capture from a Variety of Media, Application No.: 63/444,456, filed February 9, 2023.

Received: February 15, 2023 Revised: June 2, 2023 Accepted: June 23, 2023 Published: July 18, 2023

### **REFERENCES**

- Sailor, W.C., Bodansky, D., Braun, C., Fetter, S., and van der Zwaan, B. (2000). A nuclear solution to climate change? Science 288, 1177–1178. https://doi.org/10.1126/science.288. 5469.1177.
- Parsons, J., Buongiorno, J., Corradini, M., and Petti, D. (2019). A fresh look at nuclear energy. Science 363, 105. https://doi.org/10.1126/ science.aaw530.
- 3. Kaltsoyannis, N., and Liddle, S. (2016). Catalyst: nuclear power in the 21 st century. Chem 1, 659–662. https://doi.org/10.1016/j.chempr. 2016.10.003.
- 4. See: https://www.radioactivity.eu.com/site/pages/Chernobyl\_lodine\_131.htm. Last accessed on December 14th, 2022.
- Bosland, L., Dickinson, S., Glowa, G.A., Herranz, L.E., Kim, H.C., Powers, D.A., Salay, M., and Tietze, S. (2014). Iodine–paint interactions during nuclear reactor severe accidents. Ann. Nucl. Energy 74, 184–199. https://doi.org/10.1016/j.anucene.2014. 07.016.
- Zhang, X., Maddock, J., Nenoff, T.M., Denecke, M.A., Yang, S., and Schröder, M. (2022). Adsorption of iodine in metal-organic framework materials. Chem. Soc. Rev. 51, 3243–3262. https://doi.org/10.1039/ D0CS01192D.
- Xie, Y., Pan, T., Lei, Q., Chen, C., Dong, X., Yuan, Y., Shen, J., Cai, Y., Zhou, C., Pinnau, I., and Han, Y. (2021). Ionic functionalization of multivariate covalent organic frameworks to achieve an exceptionally high iodine-capture capacity. Angew. Chem. Int. Ed. Engl. 60, 22432–22440. https://doi.org/10.1002/anie. 202108522.
- Wang, P., Xu, Q., Li, Z., Jiang, W., Jiang, Q., and Jiang, D. (2018). Exceptional iodine capture in 2D covalent organic frameworks. Adv. Mater. 30, e1801991. https://doi.org/10. 1002/adma.201801991.
- Xie, W., Cui, D., Zhang, S.-R., Xu, Y.-H., and Jiang, D.-L. (2019). Iodine capture in porous organic polymers and metal-organic frameworks materials. Mater. Horiz. 6, 1571– 1595. https://doi.org/10.1039/C8MH01656A.
- Hahn, S., Alrayyani, M., Sontheim, A., Wang, X., Rominger, F., Miljanić, O.Š., and Bunz, U.H.F. (2017). Synthesis and characterization of heterobenzenacyclooctaphanes derived from cyclotetrabenzoin. Chem. Eur J. 23, 10543– 10550. https://doi.org/10.1002/chem. 201701125.

- Iyoda, M., Yamakawa, J., and Rahman, M.J. (2011). Conjugated macrocycles: concepts and applications. Angew. Chem. Int. Ed. Engl. 50, 10522–10553. https://doi.org/10.1002/anie. 201006198.
- Ōki, M. (1985). Applications of Dynamic NMR Spectroscopy to Organic Chemistry (VCH Publishers).
- Lemal, D.M., Menger, F., and Coats, E. (1964). The diazene-hydrazone rearrangement. J. Am. Chem. Soc. 86, 2395–2401. https://doi.org/10. 1021/ja01066a021.
- Ji, Q., Le, H.T.M., Wang, X., Chen, Y.-S., Makarenko, T., Jacobson, A.J., and Miljanić, O.Š. (2015). Cyclotetrabenzoin: facile synthesis of a shape-persistent molecular square and its assembly into hydrogen-bonded nanotubes. Chem. Eur J. 21, 17205–17209. https://doi.org/ 10.1002/chem.201503851.
- Barbour, L.J. (2006). Crystal porosity and the burden of proof. Chem. Commun. 1163–1168. https://doi.org/10.1039/B515612M.
- Konings, R.J.M., Wiss, T., and Beneš, O. (2015). Predicting material release during a nuclear reactor accident. Nat. Mater. 14, 247–252. https://doi.org/10.1038/nmat4224.
- Noguchi, H., and Murata, M. (1988). Physicochemical speciation of airborne <sup>131</sup>I in Japan from Chernobyl. J. Environ. Radioact. 7, 65–74. https://doi.org/10.1016/0265-931X(88) 90042-2.
- 18. Cline, J.E., Roy, P.A., Hollcroft, J.W., Houbaugh, J., McVey, T., Thomas, C.D., Pelletier, C.A., and Voilleque, P.G. (1981). Measurement of <sup>129</sup>I and Radioactive Particulate Concentrations in the TMI-2 Containment Atmosphere during and after Venting, GEND 009, UC-78; TMI Supplement.
- Tsuzuki, S., Uchimaru, T., and Mikami, M. (2006). Intermolecular interaction between hexafluorobenzene and benzene: Ab initio calculations including CCSD(T) level electron correlation correction. J. Phys. Chem. A 110, 2027–2033. https://doi.org/10.1021/ jp0544610.
- Allen, F.H., Kennard, O., Watson, D.G., Brammer, L., Orpen, A.G., and Taylor, R. (1987). Tables of bond lengths determined by X-ray and neutron diffraction. Part 1. Bond lengths in organic chemistry compounds. J. Chem. Soc. Perkin Trans. 2, S1–S9. https://doi.org/10.1039/ p298700000s1.

- Benson, S.W. (1965). III-Bond energies.
   J. Chem. Educ. 42, 502–518. https://doi.org/10. 1021/ed042p502.
- 22. Contrell, T.L. (1958). Strengths of Chemical Bonds, 2<sup>nd</sup> Ed (Butterworths).
- Mishra, B.K., Arey, J.S., and Sathyamurthy, N. (2010). Stacking and spreading interactions in N-heteroatomic systems. J. Phys. Chem. A 114, 9606–9616. https://doi.org/10.1021/ jp908941u.
- Sierański, T. (2017). Discovering the stacking landscape of pyridine-pyridine systems. J. Mol. Model. 23, 338–353. https://doi.org/10.1007/ s00894-017-3496-4.
- Ghasempour, H., Wang, K.-Y., Powell, J.A., ZareKarizi, F., Lv, X.-L., Morsali, A., and Zhou, H.-C. (2021). Metal-organic frameworks based on multicarboxylate linkers. Coord. Chem. Rev. 426, 213542. https://doi.org/10.1016/j.ccr. 2020.213542
- Moreau, F., Kolokolov, D.I., Stepanov, A.G., Easun, T.L., Dailly, A., Lewis, W., Blake, A.J., Nowell, H., Lennox, M.J., Besley, E., et al. (2017). Tailoring porosity and rotational dynamics in a series of octacarboxylate metalorganic frameworks. Proc. Natl. Acad. Sci. USA 114, 3056–3061. https://doi.org/10.1073/pnas. 1615172114
- 27. Furukawa, H., Ko, N., Go, Y.B., Aratani, N., Choi, S.B., Yazaydin, A.Ö., Yazaydin, A.O., O'Keeffe, M., O'Keeffe, M., Kim, J., and Yaghi, O.M. (2010). Ultrahigh porosity in metalorganic frameworks. Science 329, 424–428. https://doi.org/10.1126/science.1192160.
- Farha, O.K., Eryazici, I., Jeong, N.C., Hauser, B.G., Wilmer, C.E., Sarjeant, A.A., Snurr, R.Q., Nguyen, S.T., Yazaydın, A.Ö., and Hupp, J.T. (2012). Metal-organic framework materials with ultrahigh surface areas: is sky the limit? J. Am. Chem. Soc. 134, 15016–15021. https://doi.org/ 10.1021/ja3055639.
- 29. Li, P., Vermeulen, N.A., Malliakas, C.D., Gómez-Gualdrón, D.A., Howarth, A.J., Mehdi, B.L., Dohnalkova, A., Browning, N.D., O'Keeffe, M., and Farha, O.K. (2017). Bottom-up construction of a superstructure in a porousuranium-organic crystal. Science 356, 624–627. https://doi.org/10.1126/science.aam7851.
- Ma, L., Mihalcik, D.J., and Lin, W. (2009). Highly porous and robust 4,8-connected metalorganic frameworks for hydrogen storage.
   J. Am. Chem. Soc. 131, 4610–4612. https://doi. org/10.1021/ja809590n.

### Article



- 31. Wang, B., Lv, X.-L., Lv, J., Ma, L., Lin, R.-B., Cui, H., Zhang, J., Zhang, Z., Xiang, S., and Chen, B. (2019). A novel mesoporous hydrogen-bonded organic framework with high porosity and stability. Chem. Commun. 56, 66–69. https://doi.org/10.1039/C9CC07802A.
- Yin, Q., Li, Y.-L., Li, L., Lü, J., Liu, T.-F., and Cao, R. (2019). Novel hierarchical meso-microporous hydrogen-bonded organic framework for selective separation of acetylene and ethylene versus methane. ACS Appl. Mater. Interfaces 11, 17823–17827. https://doi.org/10.1021/ acsami.9b03696.
- 33. Zhang, G., Presly, O., White, F., Oppel, I.M., and Mastalerz, M. (2014). A permanent mesoporous organic cage with an exceptionally high surface area. Angew. Chem.

- Int. Ed. Engl. *53*, 1516–1520. https://doi.org/10.1002/anie.201308924.
- 34. Pulido, A., Chen, L., Kaczorowski, T., Holden, D., Little, M.A., Chong, S.Y., Slater, B.J., McMahon, D.P., Bonillo, B., Stackhouse, C.J., et al. (2017). Functional materials discovery using energy-structure-function maps. Nature 543, 657–664. https://doi.org/10.1038/nature21419.
- Luo, D., He, Y., Tian, J., Sessler, J.L., and Chi, X. (2022). Reversible iodine capture by nonporous adaptive crystals of a bipyridine cage. J. Am. Chem. Soc. 144, 113–117. https://doi.org/10. 1021/jacs.1c11731.
- He, L., Chen, L., Dong, X., Zhang, S., Zhang, M., Dai, X., Liu, X., Lin, P., Li, K., Chen, C., et al. (2021). A nitrogen-rich covalent

- organic framework for simultaneous dynamic capture of iodine and methyl iodide7, pp. 699–714.
- Li, H., Zhang, D., Cheng, K., Li, Z., and Li, P.-Z. (2023). Effective iodine adsorption by nitrogenrich nanoporous covalent organic frameworks. ACS Appl. Nano Mater. 6, 1295–1302. https://doi.org/10.1021/acsanm.2c04941.
- 38. Shao, B., and Aprahamian, I. (2020). Hydrazones as new molecular tools. Chem 6, 2162–2173. https://doi.org/10.1016/j.chempr. 2020.11.024.
- Aprahamian, I. (2017). Hydrazone switches and things in between. Chem. Commun. 53, 6674–6684. https://doi.org/10.1039/ C7CC02879B.